Bidirectional DC-DC Topologies Comparison for 800 V Automotive Applications Integrating 650 V GaN-on-Si Devices

Ilias Chorfi, Julio Brandelero, Corinne Alonso, Romain Month Éard, Thierry Sutto

▶ **To cite this version:**

Ilias Chorfi, Julio Brandelero, Corinne Alonso, Romain Month Éard, Thierry Sutto. Bidirectional DC-DC Topologies Comparison for 800 V Automotive Applications Integrating 650 V GaN-on-Si Devices. PCIM Europe 2024; International Exhibition and Conference for Power Electronics, Intelligent Motion, Renewable Energy and Energy Management, PCIM Europe, Jun 2024, Nürnberg, Germany, Germany. hal-04774982

HAL Id: hal-04774982
https://hal.science/hal-04774982v1

Submitted on 9 Nov 2024

HAL is a multi-disciplinary open access archive for the deposit and dissemination of scientific research documents, whether they are published or not. The documents may come from teaching and research institutions in France or abroad, or from public or private research centers.

L'archive ouverte pluridisciplinaire **HAL**, est destinée au dépôt et à la diffusion de documents scientifiques de niveau recherche, publiés ou non, émanant des établissements d'enseignement et de recherche français ou étrangers, des laboratoires publics ou privés.

 DOI: 10.30420/566262307

pcim EUROPE

Bidirectional DC-DC Topologies Comparison for 800 V Automotive Applications Integrating 650 V GaN-on-Si Devices

Ilias Chorfi[1], Julio Brandelero[1], Corinne Alonso[2], Romain Monthéard[3], Thierry Sutto[1]

[1] STMicroelectronics, Automotive & Discrete Group (ADG). Labège, France
[2] LAAS-CNRS, Université de Toulouse, CNRS, UPS. Toulouse, France
[3] Commissariat à l'énergie atomique et aux énergies alternatives (CEA). Labège, France.

Corresponding author: Ilias Chorfi, ilias.chorfi@st.com
Speaker: Ilias Chorfi, ilias.chorfi@st.com

Abstract

Wide band gap (WBG) devices and particularly Gallium Nitride (GaN) switches are attractive solutions to increase the compactness of power converters in automotive applications, thanks to their improved switching characteristics and lower on-resistance. Nevertheless, their 650 V voltage rating limits their use in 800 V on-board chargers (OBC). In this paper, a side-by-side comparison between two isolated 800 V dc-dc topologies is proposed, backed by consistent experimental data. These topologies are based on 650 V GaN-on-Si devices and derived from the dual active bridge (DAB): the series-input series-output dual active half bridge (SISO DAHB) topology and the three-level active neutral point clamped DAHB (3L-ANPC DAHB) topology. This work compares the trade-offs between these two power circuits and evaluates the impact of the switching frequency and transformer design on the GaN switches losses, the overall conversion efficiency, as well as thermal dissipation. Experiments conducted on the realized prototypes show very good efficiencies even at high switching frequencies. Slightly lower losses are observed in SISO DAHB compared to 3L-ANPC DAHB, that has a greater switch count but fewer passive components.

1 Introduction

Upgrading the battery voltage from 400 V to 800 V reduces the wiring harness and decreases the charging time, allowing improvement of the overall performance of electrical vehicles (EV) [1][2]. The dual active bridge isolated dc-dc topology is used in various applications, but it is particularly interesting for EV charging applications due to its high efficiency, ease of zero voltage switching (ZVS), reliability and bidirectional power flow [3][4]. The DAB topology could benefit from using GaN devices with their improved switching characteristics and lower on-resistance ($R_{DS,on}$) [5]. Furthermore, GaN devices are particularly interesting in ZVS dc-dc topologies such as DAB topology, because of their very low turn-off energy which is 10 times lower than that of Silicon Carbide (SiC) MOSFET with equivalent ratings as can be seen in Fig. 1. Thus, the switching frequency could be increased to reduce the size of the passives while maintaining good efficiency compared to SiC as shown in Fig. 2. Furthermore, thanks to the very low parasitic capacitance of the GaN devices, ZVS operation is achieved even at light loads. Nevertheless, the most commonly available and mature GaN transistors are qualified at 650 V [6].

This paper proposes a comparison between SISO DAB and multilevel DAB topologies in half-bridge configuration, used to overcome the voltage rating limitation of GaN devices in 7.4 kW/800 V battery charging systems. In section 2, the operational principle of each topology is explained, and the theoretical waveforms are provided, as well as the comparison between the two topologies. In section 3, the high frequency magnetic design is discussed. Finally, the experimental realization and results of both topologies are shown in section 4.

ISBN 978-3-8007-6262-0 © VDE VERLAG GMBH · Berlin · Offenbach
Authorized licensed use limited to: LAAS. Downloaded on November 08,2024 at 12:50:19 UTC from IEEE Xplore. Restrictions apply.

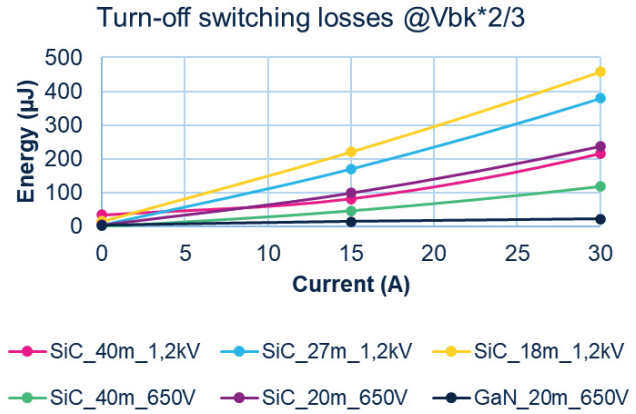

Fig. 1: Turn-off switching energies of different GaN and SiC power devices

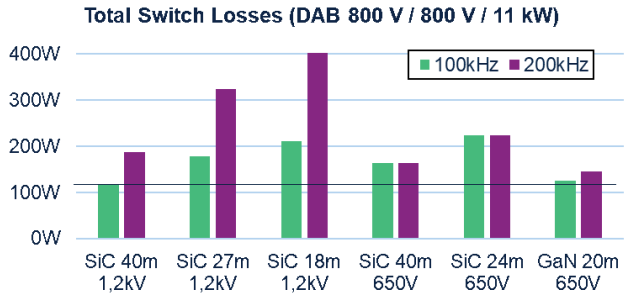

Fig. 2: Total losses for a conventional DAB different GaN and SiC power devices

2 Operation principle of the proposed topologies

The DAB topology can be implemented in different configurations while maintaining the same principle of operation [7], which consists of introducing a phase shift between the control signals of the primary and the secondary to create a power flow from the leading bridge to the lagging bridge. DAB topology is inherently bidirectional. In a full bridge configuration, any slight difference between the duty cycles of the devices can cause a DC bias current in the transformer which leads to core saturations and additional losses. This phenomenon is naturally avoided when using the dual active half bridge (DAHB) by using a capacitive voltage divider that blocks the DC current bias that leads to smaller magnetics, as they do not have to account for the DC current. Figure 3 represents the two proposed 800 V DAHB topologies using 650 V GaN devices. In Fig. 3a, two two-level DAHB converters are stacked in series to sustain 800 V, while in Fig. 3b, the half bridges of the DAHB are implemented using three-level Active Neutral Point Clamped (3L-ANPC) topology to support 800 V.

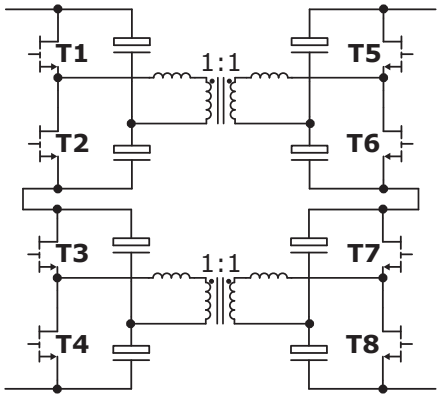

(a) SISO DAHB topology

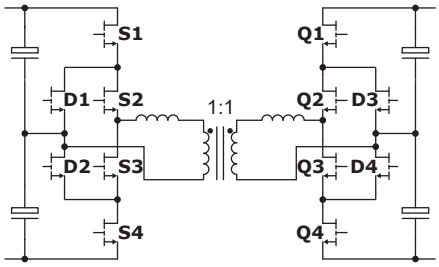

(b) 3L-ANPC DAHB topology

Fig. 3: The proposed topologies for 800 V dc-dc converter using 650 V GaN devices

Table 1 shows the technical parameters of both topologies, the same technical specifications is fixed for both topologies to have a meaningful comparison.

Parameter	Value
Input voltage (V_{in})	800 V
Output voltage (V_{out})	800 V
Output power (P_{out})	7.4 kW
Switching frequency (f_{sw})	250 kHz

Tab. 1: Technical specifications of the proposed topologies

Phase-Shifted Pulse Width Modulation (PS-PWM) is applied to the primary and secondary ANPC half-bridges in order to generate the three-level square voltage. Fig. 4 shows the gate drive signals of the different devices in the proposed converter, all devices switch at 50% duty cycle with a phase shift applied between the outer switches (S_1–S_4 and S_5–S_8) and inner switches (S_2–S_3 and S_6–S_7). The phase shift d_1 is applied to the primary half-bridge, while d_2 is applied to the secondary half-bridge. To simplify the analysis and the design of the pro-

ISBN 978-3-8007-6262-0

© VDE VERLAG GMBH · Berlin · Offenbach
Authorized licensed use limited to: LAAS. Downloaded on November 08,2024 at 12:50:19 UTC from IEEE Xplore. Restrictions apply.

posed converter, d_1 and d_2 are considered equal and are referred to as d_1 in the following. PS-PWM modulation is selected for its multiple advantages such as natural voltage balancing of the different devices, even losses distribution and ease of implementation. The natural voltage balancing is highly desirable as it eliminates the need of using sophisticated and resource-heavy active voltage balancing algorithms. The transferred power from the primary side to the secondary side is described by (1), where P_{out} is the average output power, ω is the switching angular frequency, and n is the turn ratio of the AC-link transformer. This equation is valid only in the case of $d_1 < \Phi < \frac{\pi}{2}$. The value and the direction (direct or reversed) of the transferred power can be controlled by choosing the appropriate combination of d_1 and Φ. If $d_1 = 0°$ in (1), the equation is reduced to the SISO DAHB converter as can be seen in equation (2).

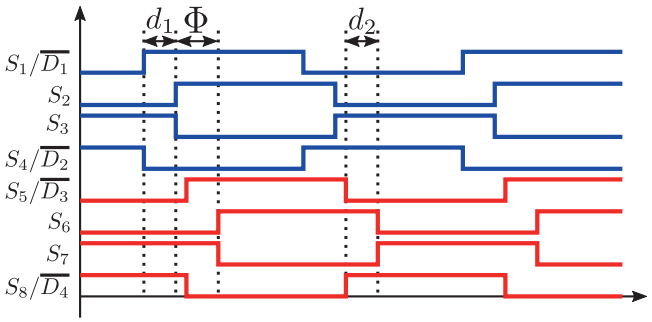

Fig. 4: PS-PWM gate drive signals applied to the three-level DAHB

$$P_{out_{3L}} = \frac{n \cdot V_p \cdot V_s}{\omega \cdot L_{lk_{3L}}} \cdot (\Phi - \frac{\Phi^2}{\pi} - \frac{d_1^2}{\pi}) \qquad (1)$$

$$P_{out_{2L}} = \frac{n \cdot V_p \cdot V_s}{\omega \cdot L_{lk_{2L}}} \cdot (\Phi - \frac{\Phi^2}{\pi}) \qquad (2)$$

Figure 5 shows the different theoretical waveforms of the three-level ANPC DAHB under the condition of $d_1 < \Phi < \frac{\pi}{2}$. This condition can be considered the generalized case [8]. The near-sinusoidal shape of the transformer current contains very few harmonics (THDi) which results in more efficient and smaller magnetics, eventually leading to greater compactness.

2.1 Comparison of the two topologies

Table 2 shows the required components and their voltage/current stress for each topology, assuming a 1:1 transformer turn ratio. SISO DAHB requires more passives which impacts the power density,

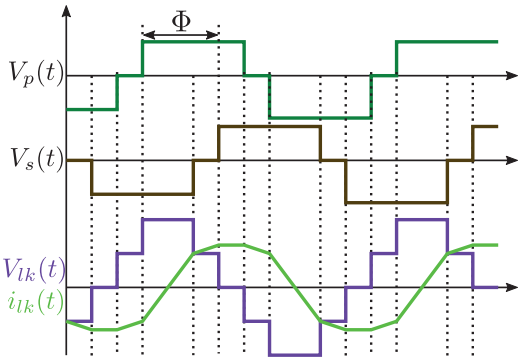

Fig. 5: Three-level DAHB converter waveforms

and may result in reliability issues compared to the 3L-ANPC topology. Furthermore, the capacitors of the SISO DAHB need an active voltage balancing algorithm in order for the converter to operate correctly, while the capacitors voltages are balanced naturally in the case of 3L-ANPC DAHB due to the use of phase-shift PWM modulation [9]. The major advantage of the SISO DAHB topology is the ability to operate at a wide voltage range, as well as its lower switch count compared to 3L-ANPC DAHB. On the other hand, 3L-ANPC DAHB requires four more GaN devices which results in more losses, however it should be noted that the D1, D2, D3 and D4 devices are clamping devices, and should theoretically present near zero losses. In practice they present low non-negligible losses since they operate at ZVS and ZCS. The major advantage of the 3L-ANPC DAHB topology is the additional voltage level in each bridge, leading to less harmonics, thus increasing the efficiency of the magnetics and reducing dv/dt and di/dt (EMI). Furthermore, the additional voltage level extends the ZVS range of the topology, especially at light loads [10], although it adds complexity to the control algorithm.

3 Transformer design

Table 3 shows the technical specifications of the transformer. In order to improve further the power density of the converter, the series power transfer inductor will be integrated in the transformer. Furthermore, the stray inter-winding capacitance is limited to 300 pF to limit the oscillations due to the fast transients of the GaN devices. The same transformer will be used for both topologies, in the case of SISO-DAHB topology, each DAHB is implemented using a 3.7 kW transformer to have 7.4 kW in total, as for the 3L-ANPC DAHB, two transformers connected in series will be used to support $\pm$400 V and 7.4 kW operation.

ISBN 978-3-8007-6262-0

© VDE VERLAG GMBH · Berlin · Offenbach
Authorized licensed use limited to: LAAS. Downloaded on November 08,2024 at 12:50:19 UTC from IEEE Xplore. Restrictions apply.

	Quantity		Current stress		Voltage stress	
	SISO DAHB	ANPC DAHB	SISO DAHB	ANPC DAHB	SISO DAHB	ANPC DAHB
GaN devices	8	12	$2I_{out}$	$2I_{out}$	$V_{bus}/2$	$V_{bus}/2$
Transformer	2	1	$2I_{out}$	$2I_{out}$	$V_{bus}/4$	$V_{bus}/2$
Capacitor	8	4	N/A	N/A	$V_{bus}/4$	$V_{bus}/2$
Inductor	4	2	$2I_{out}$	$2I_{out}$	N/A	N/A

Tab. 2: Comparison of different active and passive elements of SISO and 3L-ANPC DAHB topology

Parameter	Value
Turn ratio	1:1
f_{sw}	250 kHz
Input/output voltage	$\pm$200 V
Peak current	22 A_{pk}
RMS current	20 A_{RMS}
Nominal power	3.7 kW
Magnetizing inductance	100 µH
Total leakage	4.2 µH
Stray inter-winding capacitance	$\leq$300 pF

Tab. 3: Technical specifications of the high frequency transformer

The transformer is constructed using two PQ60/52 cores in KF9A material for the transformer, and one PQ60/52 core for the inductor. The inductor core is fitted on the top of the transformer cores to improve magnetic coupling and to better control the value of the leakage inductor. In addition, the winding are realized using six 660x0.05mm Litz wire in parallel to support the high RMS current at the high switching frequency. Figure 6 shows the realized 3.7 kW/250 kHz transformer.

Fig. 6: The experimental realization of the high frequency transformer

4 Experimental results

The two converters are constructed using a modular approach. Each pair of devices is implemented in a daughterboard using 25 mΩ top-cooled GaN HEMTs in a PFLAT8x8 package, with a bus bar motherboard PCB ensuring the appropriate connections for each topology. The GaN devices are assembled on the bottom of the board to take advantage of the top side cooling, as seen in Fig. 7, where the heatsink is a 60 °C cold plate.

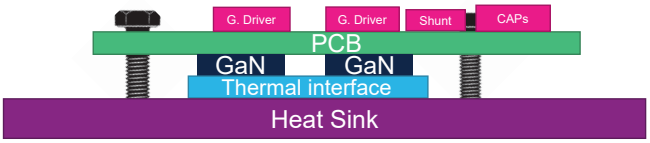

Fig. 7: Mechanical assembly of the GaN daughterboards

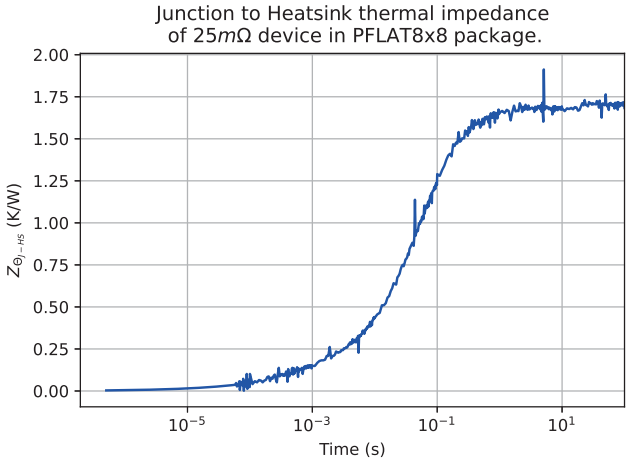

Fig. 8: Junction-to-heatsink thermal impedance of the 25 mΩ GaN device in PFLAT8x8 using GP5000S35 TIM

Figure 9 shows the experimental prototypes of the proposed topologies, the transformer is not assembled in the pictures. The experimental waveforms of both topologies are presented in Fig. 10, the current shape of the 3L-ANPC DAHB topology is nearly sinusoidal which result in lower THDi and better EMI performances. Furthermore, the addi-

ISBN 978-3-8007-6262-0

© VDE VERLAG GMBH · Berlin · Offenbach
Authorized licensed use limited to: LAAS. Downloaded on November 08,2024 at 12:50:19 UTC from IEEE Xplore. Restrictions apply.

tionnal voltage level reduce the dv/dts. The waveforms in both topologies have minimal oscillations and overshoot due to the optimized layout of the GaN daughterboards, and the small inter-winding stray capacitance of the transformer.

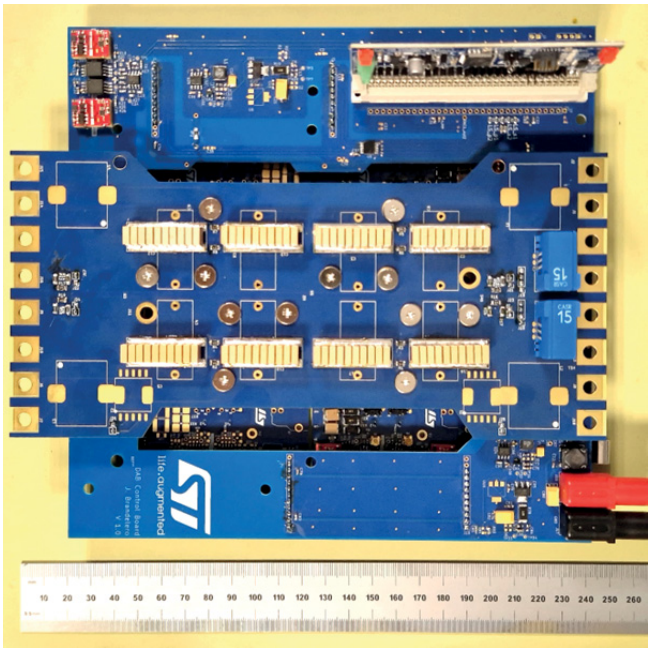

(a) SISO DAHB experimental prototype

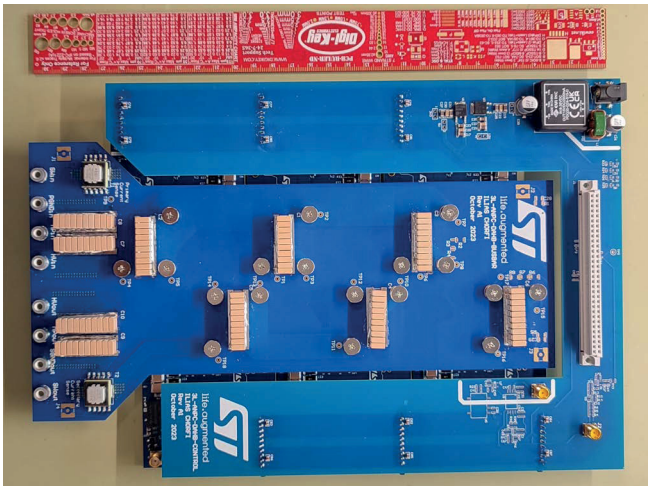

(b) 3L-ANPC DAHB experimental prototype

Fig. 9: Experimental prototypes of the proposed topologies

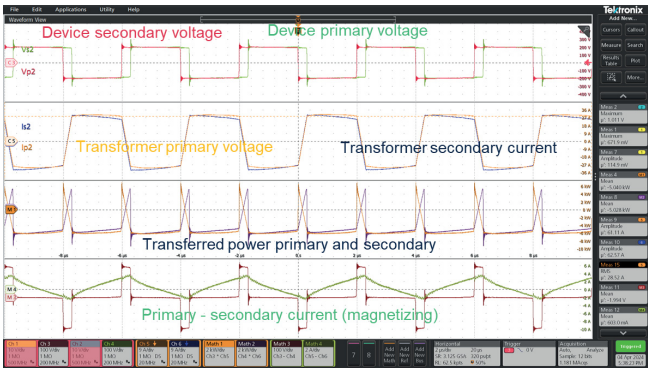

(a) SISO DAHB experimental waveforms

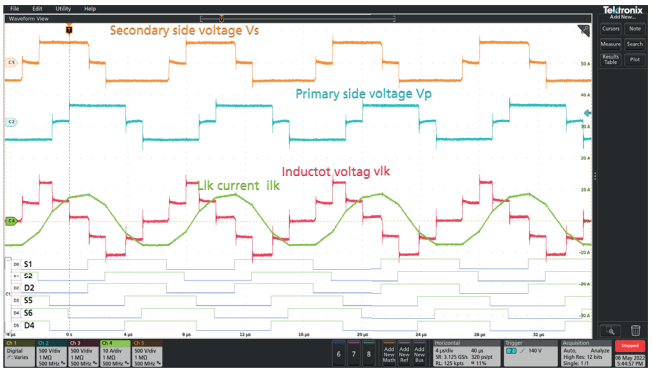

(b) 3L-ANPC DAHB experimental waveforms

Fig. 10: Experimental waveforms of the proposed topologies

The efficiency of both realized converters is measured at $V_{in=out}$=800 V and for cold plate temperature of 20 °C and 60 °C as can be seen in Fig. 11. The temperature of the cold plate has very little effect on the efficiency of both converter up to the rated power of 7.4 kW. However, when the output power is higher than the rated power, the 20 °C cold plate allows the operation of both converters upto to 10 kW while maintaining a good efficiency of about 97%. While the 60 °C cold plate limit the operation to 8 kW.

The efficiency of the 3L-ANPC DAHB converter is slightly less than that of the SISO DAHB converter, due to the additionnal clamping devices in the 3L-ANPC DAHB converter, which they add about 1.5 W of losses per devices on the entire power range. The clamping devices operates at ZVS and ZCS and zero RMS current, therefore, the losses of these devices are due to other mechanisms such as deadtime and associated third-quandrant losses.

When the output power is less than 1 kW,

ISBN 978-3-8007-6262-0

© VDE VERLAG GMBH · Berlin · Offenbach
Authorized licensed use limited to: LAAS. Downloaded on November 08,2024 at 12:50:19 UTC from IEEE Xplore. Restrictions apply.

all the devices operates at hard-switching in both converters which explain the low efficiency. However, the moment the devices operates in ZVS, the efficiency is quite flat on the remaining power range due to the very low turn-off energy of GaN devices.

Figure 12 shows the thermal imagery of the realized transformer at the rated power of 3.7 kW, the hot spot is measured at 94 °C with natural cooling, which is reasonable for automotive applications. The thermal imagery shows a well balanced temperature gradient between the copper and the core. Furthermore, the transformer will be capable of passing more power if is cooled by the same cold plate used for the GaN devices.

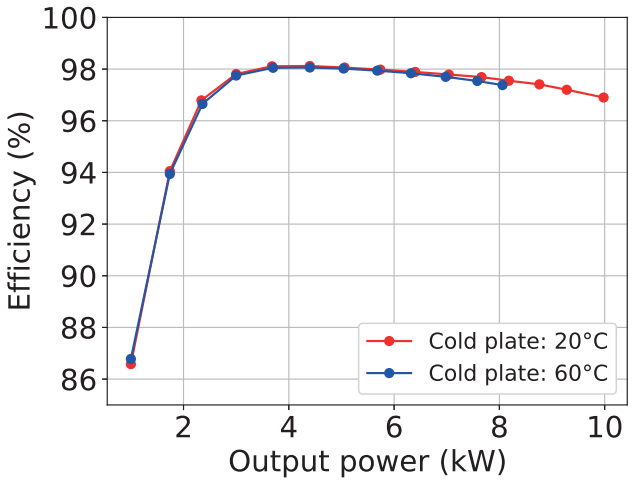

(a) Efficiency of SISO-DAHB at 800 V

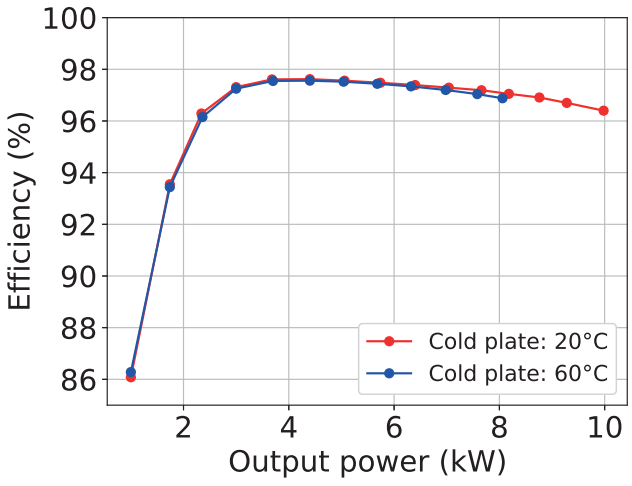

(b) Efficiency of 3L-ANPC DAHB at 800 V

Fig. 11: Efficiency of the realized converters at 250 kHz

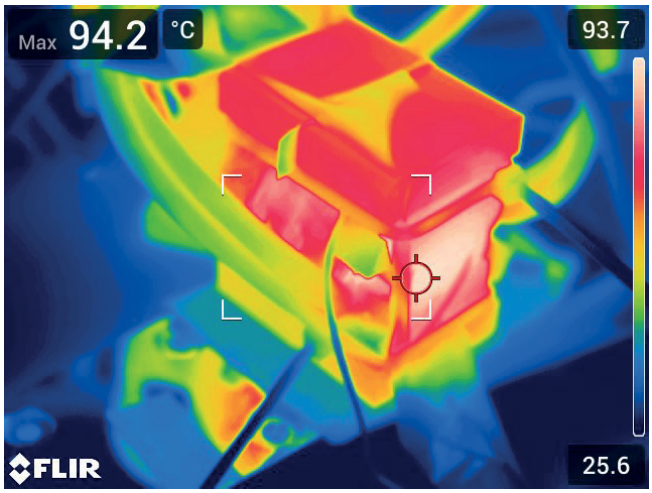

Fig. 12: Thermal image of the transformer at the maximum power

5 Conclusion

With a focus on providing side-by-side GaN-based experimental data, this article proposed a fair comparison of the SISO DAHB and the 3L-ANPC DAHB, which are derived from the well-known two-level DAB topology. Both can be proposed as a solution to enable the use of 650 V GaN devices in 800 V/11 kW battery charging systems for EVs. The topologies take full advantage of the low GaN turn-off energy to achieve a very good efficiency, even when operating at 1 MHz switching frequency. The SISO topology shows slightly better efficiency due to its lower switch count. The 3L-ANPC DAHB has fewer magnetics and capacitors and can therefore be expected to achieve greater power density and reliability

References

[1] C. Jung, “Power up with 800-v systems: The benefits of upgrading voltage power for battery-electric passenger vehicles,” *IEEE Electrification Magazine*, vol. 5, no. 1, pp. 53–58, 2017. DOI: 10.1109/MELE.2016.2644560.

[2] M. Safayatullah, M. T. Elrais, S. Ghosh, R. Rezaii, and I. Batarseh, “A comprehensive review of power converter topologies and control methods for electric vehicle fast charging applications,” *IEEE Access*, vol. 10, pp. 40 753–40 793, 2022. DOI: 10.1109/ACCESS.2022.3166935.

[3] B. Zhao, Q. Song, W. Liu, and Y. Sun, “Overview of dual-active-bridge isolated bidirectional dc–dc converter for high-frequency-link power-conversion system,” *IEEE Transactions on Power Electronics*, vol. 29, no. 8, pp. 4091–4106, 2014. DOI: 10.1109/TPEL.2013.2289913.

Authorized licensed use limited to: LAAS. Downloaded on November 08,2024 at 12:50:19 UTC from IEEE Xplore. Restrictions apply.

[4] P. He and A. Khaligh, "Comprehensive analyses and comparison of 1 kw isolated dc–dc converters for bidirectional ev charging systems," *IEEE Transactions on Transportation Electrification*, vol. 3, no. 1, pp. 147–156, 2017. DOI: 10.1109/TTE.2016.2630927.

[5] J. Millán, P. Godignon, X. Perpiñà, A. Pérez-Tomás, and J. Rebollo, "A survey of wide bandgap power semiconductor devices," *IEEE Transactions on Power Electronics*, vol. 29, no. 5, pp. 2155–2163, 2014. DOI: 10.1109/TPEL.2013.2268900.

[6] S. Chowdhury, Y. Wu, L. Shen, P. Smith, J. Gritters, *et al.*, "650 v highly reliable gan hemts on si substrates over multiple generations: Expanding usage of a mature 150 mm si foundry," in *2019 30th Annual SEMI Advanced Semiconductor Manufacturing Conference (ASMC)*, 2019, pp. 1–5. DOI: 10.1109/ASMC.2019.8791814.

[7] H. Higa, S. Takuma, K. Orikawa, and J.-i. Itoh, "Dual active bridge dc-dc converter using both full and half bridge topologies to achieve high efficiency for wide load," in *2015 IEEE Energy Conversion Congress and Exposition (ECCE)*, 2015, pp. 6344–6351. DOI: 10.1109/ECCE.2015.7310549.

[8] M. A. Moonem, C. L. Pechacek, R. Hernandez, and H. Krishnaswami, "Analysis of a multilevel dual active bridge (ml-dab) dc-dc converter using symmetric modulation," *Electronics*, vol. 4, no. 2, pp. 239–260, 2015. DOI: 10.3390/electronics4020239.

[9] Y. Li, H. Tian, and Y. W. Li, "Generalized phase-shift pwm for active-neutral-point-clamped multilevel converter," *IEEE Transactions on Industrial Electronics*, vol. 67, no. 11, pp. 9048–9058, 2020. DOI: 10.1109/TIE.2019.2956372.

[10] Y. Ikai and N. Hoshi, "Expanding zvs range for dual active bridge dc-dc converter using three-level neutral-point-clamped inverter topology," in *2016 IEEE International Conference on Renewable Energy Research and Applications (ICRERA)*, 2016, pp. 472–477. DOI: 10.1109/ICRERA.2016.7884382.

ISBN 978-3-8007-6262-0 © VDE VERLAG GMBH · Berlin · Offenbach
Authorized licensed use limited to: LAAS. Downloaded on November 08,2024 at 12:50:19 UTC from IEEE Xplore. Restrictions apply.